

Earlier springs are causing reduced nitrogen availability in North American eastern deciduous forests

Andrew J. Elmore^{1*}, David M. Nelson¹ and Joseph M. Craine²

There is wide agreement that anthropogenic climate warming has influenced the phenology of forests during the late twentieth and early twenty-first centuries^{1,2}. Longer growing seasons can lead to increased photosynthesis and productivity³, which would represent a negative feedback to rising CO₂ and consequently warming^{4,5}. Alternatively, increased demand for soil resources because of a longer photosynthetically active period in conjunction with other global change factors might exacerbate resource limitation^{6,7}, restricting forest productivity response to a longer growing season^{8,9}. In this case, increased springtime productivity has the potential to increase plant nitrogen limitation by increasing plant demand for nitrogen more than nitrogen supplies, or increasing early-season ecosystem nitrogen losses^{10,11}. Here we show that for 222 trees representing three species in eastern North America earlier spring phenology during the past 30 years has caused declines in nitrogen availability to trees by increasing demand for nitrogen relative to supply. The observed decline in nitrogen availability is not associated with reduced wood production, suggesting that other environmental changes such as increased atmospheric CO₂ and water availability are likely to have overwhelmed reduced nitrogen availability. Given current trajectories of environmental changes, nitrogen limitation is likely to continue to increase for these forests, possibly further limiting carbon sequestration potential.

A critical question for predicting the magnitude of future warming under different emissions scenarios is the degree to which forest productivity responds to longer growing seasons in the face of concurrent changes in other drivers of productivity⁴. The spring onset of greenness and autumn offset of greenness observed from remote sensing provides a consistent annual observation that is related to the beginning and end of annual carbon uptake for temperate forests, which is a strong predictor of forest productivity³. Relative to the beginning of the remote sensing record in the early 1980s, climate warming has driven both advanced spring onset and delayed autumn offset in temperate deciduous forests of North America. However, the expected productivity response to this lengthening of the growing season might be offset, for example, by increases in ecosystem respiration⁸ or by reduced resource availability³. Long-term direct measurements are not yet available to specifically address this question, but advances in remote sensing and dendroecological methods present opportunities to acquire information retrospectively to advance understanding of how phenological changes and resource availability to trees have been affecting forest productivity.

We assembled a 30-year record of remotely sensed forest phenology (30 m resolution), the isotopic composition of nitrogen and

carbon in tree rings and annual wood production of trees at 113 sites located in four study regions in the eastern United States spanning more than 500 km (Methods; Supplementary Fig. 1). The remotely sensed fraction of photosynthetic vegetation (f_{PV}) was quantified from a temporal stack of >240 Landsat TM and ETM+ scenes covering the period 1984–2013. These data were used to parameterize a dual sigmoid logistic growth curve (Supplementary Fig. 2) representing seasonal patterns of f_{PV} from which phenological parameters including spring onset and autumn offset were derived¹². The isotopic ratio of nitrogen ($\delta^{15}N$) and isotopic discrimination of carbon ($\Delta^{13}C$) were acquired for 222 trees of three deciduous species at the 113 sites. As shown for foliar $\delta^{15}N$, elevated wood $\delta^{15}N$ values indicate greater nitrogen availability to trees, defined as the supply of nitrogen relative to its demand by plants^{13–15}. Elevated wood $\Delta^{13}C$ signifies greater increases in intercellular CO₂ concentrations (C_i) than atmospheric CO₂ concentrations (C_a), which is caused by increased isotopic fractionation because of either greater stomatal conductance and/or lower photosynthetic assimilation rates in C₃ plants¹⁶.

From phenology observations made from 1984 to 2013, across sites, spring onset commenced between day of year (DOY) 117 and 144 (mean = 129) and autumn offset commenced between DOY 286 and 308 (mean = 298). In general, sites with an earlier spring onset had a later autumn offset ($r = -0.63$, $P < 0.001$; Supplementary Fig. 3). We quantified site-specific annual anomalies in spring and autumn phenology, which are the temporal deviations in a given year from the mean spring onset and the mean autumn offset, respectively¹⁷. Across all sites, by 2013 spring onset arrived on average 4.8 ± 0.5 days earlier (Supplementary Table 1 and Supplementary Fig. 4) and autumn offset arrived 2.5 ± 0.5 days later (Supplementary Table 2 and Supplementary Fig. 5) than 1984. Although the growing season lengthened by 4.3% (7.3 d) throughout the 30-year period, increases in f_{PV} during the early growing season were offset by decreases in the late growing season f_{PV} (Fig. 1), leading to just a 2.1% increase over time in the combined magnitude and duration of vegetation cover.

Tree-ring $\delta^{15}N$ values reveal that 65% of trees in the four regions have experienced declines in nitrogen availability. From 1984 to 2013, across all measured trees, wood $\delta^{15}N$ declined on average $0.44 \pm 0.08\text{‰}$ ($P < 0.001$; Supplementary Table 4), similar to the degree of reduction in $\delta^{15}N$ that has been measured previously in other trees in the region during this time¹⁴. To assess whether the decline in $\delta^{15}N$ was influenced by changes in phenology, we ran regression models of the $\delta^{15}N$ of individual rings with year and either spring or autumn anomalies as model effects. Years and sites with earlier spring onsets had lower wood $\delta^{15}N$ ($P = 0.03$; Fig. 3a and Supplementary Table 4). Later autumn offset did not

¹Appalachian Laboratory, University of Maryland Center for Environmental Science, Frostburg, Maryland, 21532, USA. ²Jonah Ventures, Manhattan, Kansas 66502, USA. *e-mail: aelmore@umces.edu

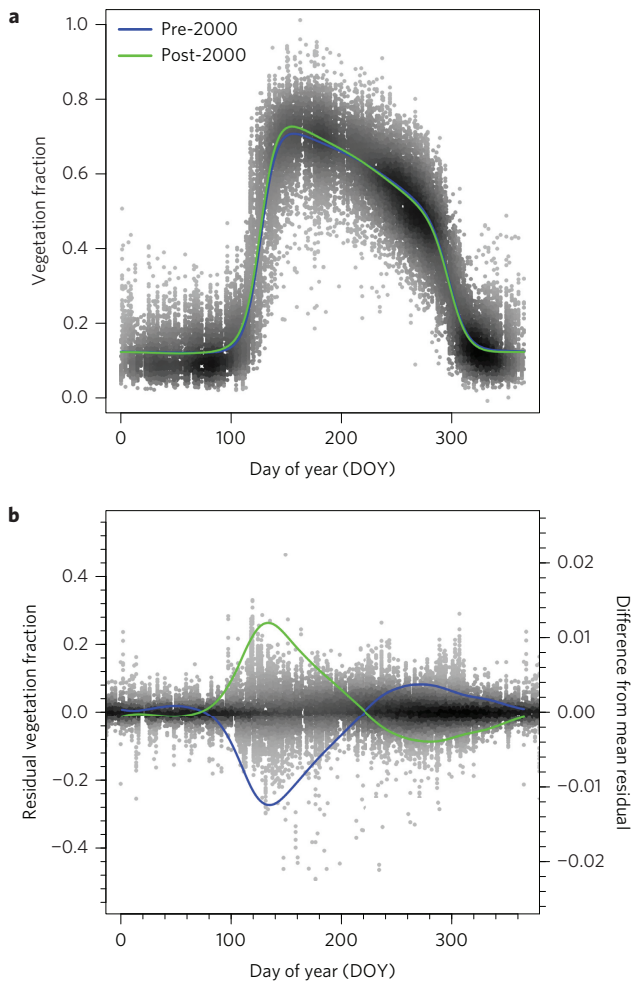


Figure 1 | Vegetation fractions using pre- and post-2000 data. **a**, The mean phenology of vegetation fraction. **b**, The mean residual vegetation fraction. Years with an early spring phenology were more common after the year 2000 and these early spring onset years are associated with increased vegetation fraction before day 220 and decreased vegetation fraction after day 220.

significantly affect $\delta^{15}\text{N}$ ($P=0.07$; Supplementary Table 6). The decline in $\delta^{15}\text{N}$ associated with earlier springs represents reduced nitrogen availability, which is not likely to be due to greater rates of gaseous nitrogen loss from soils, as this process would lead to ^{15}N enrichment of the remaining available nitrogen pool and consequently the wood of plants that rely on it¹³. Instead, the earlier spring is likely to have increased plant nitrogen demand beyond nitrogen supply rates leading to a decline in nitrogen availability and a decline in the relative fraction of gaseous nitrogen lost (Fig. 2).

Tree-ring $\Delta^{13}\text{C}$ values reveal that discrimination against ^{13}C has increased over time despite later autumns, which independently reduced discrimination against ^{13}C . In general, from 1984 to 2013, wood $\delta^{15}\text{N}$ declined, but wood $\Delta^{13}\text{C}$ increased on average $0.53 \pm 0.05\text{‰}$ ($P < 0.001$; Fig. 3b and Supplementary Table 6). However, $\Delta^{13}\text{C}$ was lower in years when autumn was later ($P < 0.001$, Supplementary Fig. 6 and Supplementary Table 7). The interpretation is that even after accounting for the reduced $\Delta^{13}\text{C}$ associated with reduced water availability during years with later autumns, wood $\Delta^{13}\text{C}$ still increased over time ($P < 0.001$; Fig. 2 and Supplementary Table 7). The decline in $\delta^{15}\text{N}$ and increase in $\Delta^{13}\text{C}$ signifies that as nitrogen availability declined, trees experienced reduced photosynthetic assimilation, increased stomatal conductance or both¹⁸. Despite the increase in discrimination against

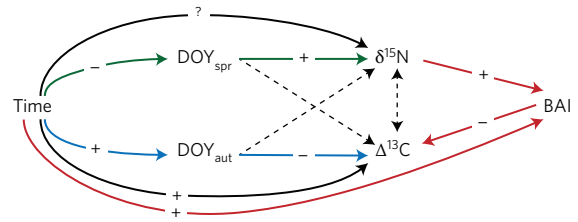


Figure 2 | Path diagram illustrating relationships between time, spring (DOY_{spr}) and autumn (DOY_{aut}) phenology, wood production (BAI), nitrogen availability ($\delta^{15}\text{N}$) and discrimination against ^{13}C ($\Delta^{13}\text{C}$). Solid lines denote significant effects. Black arrows: independent of changes in phenology, $\Delta^{13}\text{C}$ is increasing over time. However, our analyses were inconclusive as to whether nitrogen availability is declining over time independent of changes in phenology. Green arrows: earlier spring timing leads to a reduction in nitrogen availability. Blue arrows: increased $\Delta^{13}\text{C}$ (increased stomatal conductance and/or decreased photosynthetic assimilation) is observed over time; however, the effect of later autumns is to decrease discrimination, suggesting greater water limitation in these years. Red arrows: wood production (BAI) has increased over time despite declining $\delta^{15}\text{N}$, which has had the effect of decreased discrimination as water availability is reduced.

^{13}C , increased atmospheric CO_2 concentrations were large enough such that trees still experienced greater intrinsic water use efficiency (iWUE; Supplementary Fig. 7), which is defined as the ratio of photosynthesis to stomatal conductance¹⁹. In a multiple regression with data from individual trees, neither the slope of wood $\Delta^{13}\text{C}$ nor iWUE over time at a given site predicted the corresponding slope of wood $\delta^{15}\text{N}$ over time ($P > 0.35$ for both; Supplementary Tables 8 and 9). Therefore, despite trajectories of $\delta^{15}\text{N}$ and $\Delta^{13}\text{C}$ over time averaged across all sites (Fig. 3b), nitrogen limitation was apparently not driving greater discrimination through reduced photosynthetic assimilation.

Given the declines in nitrogen availability and late summer greenness, increases in discrimination against ^{13}C and the lengthening growing season exhibited at our sites, we examined how wood productivity of the sampled trees responded to the simultaneous changes in these factors. As a metric of wood production, we measured basal area increment (BAI), which is the area of wood produced at breast height each year²⁰. On average, BAI of individual trees increased $19 \text{ mm}^2 \text{ y}^{-1}$ ($P < 0.001$; Supplementary Table 10), but the slope of BAI over time varied from -88 to $149 \text{ mm}^2 \text{ y}^{-1}$ among the trees sampled. Neither earlier spring nor later autumn appeared to be associated with greater wood productivity among tree rings ($P = 0.05$ for both; Supplementary Tables 11 and 12). Although across all measurements greater $\delta^{15}\text{N}$ was associated with greater BAI ($P < 0.001$; Supplementary Table 13), individual trees with the greatest rates of decline in $\delta^{15}\text{N}$ did not have the greatest declines in BAI over time ($P = 0.08$; Supplementary Table 14). In contrast, increases in BAI were greatest for trees that showed the greatest increases in iWUE ($P = 0.004$; Supplementary Table 15). Given the correspondence between BAI and wood $\delta^{15}\text{N}$, it is likely that individual trees that are exhibiting greater increases in wood production are putting more demand on soil water than trees that are declining in productivity, thus increasing iWUE.

Increasing wood productivity in the face of declining nitrogen availability indicates that productivity in these forests is not solely nitrogen limited²¹. Based on global gradients of $[\text{N}]$ and $\delta^{15}\text{N}^{15}$ and correspondence between wood and foliar $\delta^{15}\text{N}^{15}$, the observed reduction in $\delta^{15}\text{N}$ would be expected to reduce foliar nitrogen concentrations by 0.9 mg g^{-1} , which would reduce photosynthetic rates by 4.6% for a leaf that began at 20 mg g^{-1} in 1984. This small reduction in photosynthesis from lower nitrogen availability is likely to be more than counteracted by an increase in photosynthesis

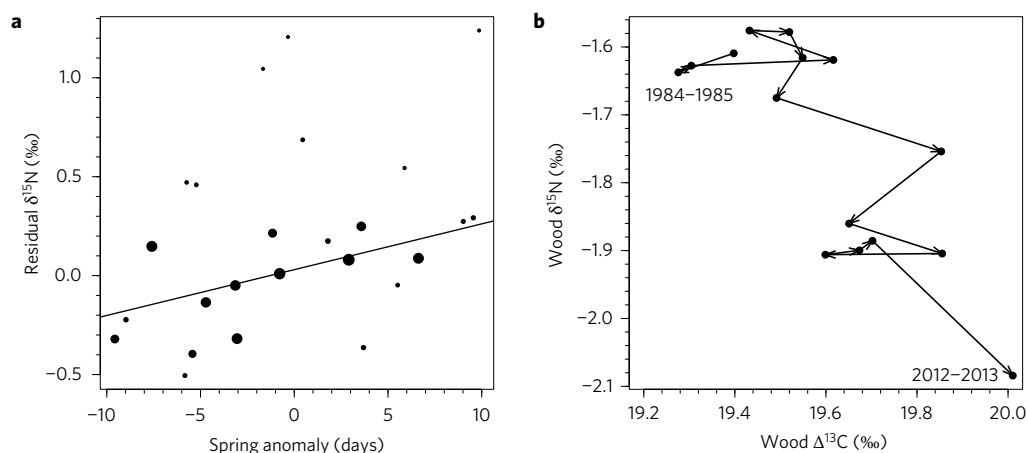


Figure 3 | Relationships between mean $\delta^{15}\text{N}$, $\Delta^{13}\text{C}$, and spring anomaly. **a**, Years exhibiting an early spring phenology anomaly are associated with low $\delta^{15}\text{N}$ ($r^2 = 0.21$; $P = 0.02$), after accounting for region and species effects. Symbol sizes represent sample sizes of paired $\delta^{15}\text{N}$ and spring anomaly observations in each year, which range from 2 to 93. **b**, Averaged biennially across all 222 trees, $\Delta^{13}\text{C}$ has increased and $\delta^{15}\text{N}$ has decreased over time.

resulting from the 15% increase in atmospheric CO_2 between 1984 and 2013. Yet, elevated atmospheric CO_2 cannot explain all the observed isotopic and productivity patterns as elevated atmospheric CO_2 generally leads to stomatal closure²². Greater stomatal closure should decrease plant $\Delta^{13}\text{C}$, not increase it¹⁹. Given that 50% of trees sampled were experiencing both increasing BAI and apparent relative water availability ($\Delta^{13}\text{C}$ was increasing) another factor must be contributing to observed patterns. Potentially contributing to greater wood productivity and increasing $\Delta^{13}\text{C}$, from 1984–2013, across the 113 sites, mean annual precipitation increased by 8% ($P < 0.001$), mean annual temperatures increased by 0.5°C ($P < 0.001$; Supplementary Fig. 8) and nitrogen deposition declined by 33%²³. Of these factors, increasing precipitation could increase both $\Delta^{13}\text{C}$ and wood production, as long as increases in temperature did not decrease soil moisture through enhanced evapotranspiration.

In all, the pattern of an earlier, longer growing season, declining $\delta^{15}\text{N}$, increasing $\Delta^{13}\text{C}$, greater productivity and reduced vegetation cover in the later half of the summer is consistent with the hypothesis that nitrogen availability is declining over time as a result of spring arriving earlier (Fig. 2). Earlier springs are likely to lead to a short-term increase in nitrogen mineralization as soils warm^{10,11}, but declining wood $\delta^{15}\text{N}$ suggests that the net effect of warming is for biotic demand to outpace nitrogen supply, leading to declining nitrogen availability. This finding stands in stark contrast to the idea that a biogeochemical planetary boundary has been crossed causing eutrophication of ecosystems globally²⁴. Yet, the patterns are congruent with modelling results that project increased discrepancies between plant demand and nitrogen supply as global temperatures and CO_2 concentrations increase⁹. Declining wood $\delta^{15}\text{N}$ is also supported by declines in nitrogen mineralization²⁵, stream nitrate export²³ and foliar nutrient concentrations including nitrogen²⁶ in temperate forests in recent decades. Overall, it is clear that the future productivity of these forests is being influenced by a matrix of changes²⁷. Other factors, such as rising CO_2 and increased precipitation, overwhelm the effect of declining nitrogen availability, causing increased net productivity and likely carbon sinks. Whether productivity and carbon storage rates will eventually decline as a result of the declining nitrogen availability will depend in part on how the phenology of forests and soil nitrogen supplies respond to future warming in conjunction with the trajectories of other global change factors affecting forests.

Methods

Remote sensing of phenology. Landsat scenes (>240 depending on location; TM and ETM+, 30 m pixel⁻¹) were processed to reflectance using the Landsat Ecosystem

Disturbance Processing System (LEDAPS²⁸), and analysed for the photosynthetic vegetation fraction, f_{PV} , using spectral mixture analysis and image endmembers²⁹. Observations of f_{PV} were organized by DOY and fit with two sigmoid logistic growth curves, one increasing in spring and a second decreasing in autumn¹². The seven parameters from these curves describe all aspects of f_{PV} phenology, including spring onset and autumn offset of greenness, averaged over the period spanned by the Landsat observations used to fit the curve (Supplementary Fig. 2). To evaluate changes in phenology, spring and autumn scenes were identified that were positioned within 20 days of the spring and autumn inflection points, greater than 20% of the site average annual minimum f_{PV} , and less than 20% (spring) and 40% (autumn) of the maximum f_{PV} . These spring- and autumn-timed Landsat observations of f_{PV} were compared against the 30-year average date of spring onset and autumn offset, respectively, to calculate anomalies. For any given location, between 5 and 16 spring f_{PV} observations and 7 and 18 autumn f_{PV} observations were identified (mean of 9.7 and 13.4, respectively)¹⁷.

We also calculated the residual vegetation cover after accounting for the mean vegetation phenology (residual in the y -direction in Fig. 1a). A spline (d.f. = 20) was fit through the residuals using three sets of data: (1) all data from all sites 1984–2013 (all data), (2) observations acquired before and including the year 2000 (pre-2000); and observations acquired after the year 2000 (post-2000). The all data spline was subsequently subtracted from the pre-2000 spline and the post-spline, respectively, and plotted to illustrate contrast between pre- and post-2000 vegetation observations to residual vegetation cover. Owing to strong annual variability in the spring onset DOY, some years with an early spring onset (the negative spring onset anomaly, described earlier) occurred pre-2000 and some years with a late spring onset occurred post-2000. Therefore, we also used the same technique described above to plot splines for vegetation residuals in years with an early and late spring, respectively (Supplementary Fig. 9). Note that although the autumn offset occurs slightly later in the season, the vegetation cover at this time of year declined from 1984 to 2013.

Field methods. Four National Parks were identified for analysis: Prince William Forest Park (PRWI; $38^\circ 35' 6''$, $-77^\circ 27' 50.4''$), Harpers Ferry Historical Park (HAFE; $39^\circ 19' 4.8''$, $-77^\circ 45' 32.4''$), Catoctin Mountain Park (CATO; $39^\circ 39' 10.8''$, $-77^\circ 27' 50.4''$) and Great Smoky Mountains Park (GRSM; $35^\circ 36' 43.2''$, $-83^\circ 29' 20.4''$) (Supplementary Fig. 1). These parks, referred to as 'regions' in this paper are within the Appalachian Oak sub-region of the mesophytic forest region extending from New England to Tennessee. The mean annual temperature is 11.76°C and the mean annual precipitation is 1,595 mm across the sampling regions. Elevation ranges from 30 m to more than 1,400 m, which influences temperature and precipitation patterns. Maps of average phenology were used to stratify and randomly select locations for tree coring within each park. An ISODATA clustering algorithm was used to identify 20 phenology classes that differed primarily in growing season length and the amplitude of annual f_{PV} . The standard deviation in phenology parameters (3×3 pixel neighbour rule) was also calculated and used to further constrain the extent of each phenology class to areas of low spatial variability in phenology. Six randomly located sites were then identified in each phenology class. Alternative sites for each phenology class were also identified; if trees of the target species were not identified at any given site an alternative site was used. Similar methods were employed at all park units used in the study; however, at GRSM we applied two further constraints that (1) all sites must be located below 1,400 m to ensure access to trees of the target species, and (2) sites were located within 250 m of a designated trail to facilitate site access. One hundred and twenty sites were initially identified (60 at northern parks (PRWI, HAFE, and CATO) and

60 at GRSM), but because of access and the availability of the target species only 113 were ultimately included in the study.

At each site, we targeted for coring the two largest specimens (occupying the largest portion of the canopy) of three species: *Quercus alba* (QUAL), *Quercus rubra* (QURU) or *Liriodendron tulipifera* (LITU). Although each species exhibits habitat preferences, all three are common across the study region. If only one of the three species was present, we cored two trees of the same species. Across all 113 sites, we cored 222 trees using a 5.15 mm diameter increment borer at ~1.4 m (breast height) above the forest floor. Two cores positioned at right angles to each other were extracted and stored in paper straws. The species and diameter at breast height (DBH) were recorded.

Analytical measurements. The cores were dried at 60 °C for at least 48 hours, sanded, and then scanned at 472 dots per centimetre. The images were analysed for ring width using Cytis CDendro Software (Saltsjobaden) and ages assigned to each ring following close visual examination of the increment core. To ensure data quality, we visually cross-dated cores from the same tree and trees from the same site using plots of normalized ring widths and, for a subset of cores, had a second researcher collect ring coordinates. One core from each tree was sectioned into annual increments using a razor blade. Approximately 1 mg of wood from each increment from each core was analysed for $\delta^{13}\text{C}$ using a Carlo Erba NC2500 elemental analyser (CE Instruments) interfaced with a ThermoFinnigan Delta V+ isotope ratio mass spectrometer (IRMS). Approximately 10 mg of wood from alternate increments was analysed for $\delta^{15}\text{N}$ using the same instruments. Alternate increments were sampled to limit any effects of nitrogen mobility that might have occurred between adjacent tree rings. However, in general, nitrogen mobility is not a large concern based on experiments utilizing an artificial tracer that have shown limited nitrogen mobility (~1 year) between tree rings less than 30 years old. For $\delta^{13}\text{C}$ analysis, a MgClO_4 trap was used to remove water vapour before the transfer of sample gases to the IRMS, whereas for $\delta^{15}\text{N}$ analysis a Carbosorb trap was used to remove CO_2 in advance of removing water vapour with MgClO_4 . The $\delta^{13}\text{C}$ and $\delta^{15}\text{N}$ data were normalized to the VPDB and AIR scales, respectively, using a two-point normalization curve with internal standards calibrated against USGS40 and USGS41. Analytical precision (1 σ) of an internal wood standard analysed alongside samples was 0.1‰ for $\delta^{13}\text{C}$ and 0.3‰ for $\delta^{15}\text{N}$.

Carbon isotopes were normalized for trends in atmospheric $\delta^{13}\text{C}$ resulting from fossil fuel use to arrive at carbon isotope discrimination against ^{13}C ($\Delta^{13}\text{C}$)³⁰.

$$\Delta^{13}\text{C} = \frac{\delta^{13}\text{C}_{\text{air}} - \delta^{13}\text{C}_{\text{wood}}}{1 + \delta^{13}\text{C}_{\text{wood}}/1000}$$

where $\delta^{13}\text{C}_{\text{wood}}$ is the measured $\delta^{13}\text{C}$ in tree rings and $\delta^{13}\text{C}_{\text{air}}$ are seasonally integrated $\delta^{13}\text{C}$ measured in the atmosphere at Mauna Loa, Hawaii, 1984–2013. $\Delta^{13}\text{C}$ is used throughout the paper and in all statistical analyses. The Mauna Loa record also provides time series of atmospheric CO_2 concentration (C_a), which were used to calculate the iWUE³⁰:

$$\text{iWUE} = 0.625 \cdot C_a \left(1 - \frac{\Delta^{13}\text{C} - a}{b - a}\right)$$

where the constant a arises from fractionation of CO_2 during diffusion through stomata (4.4‰) and b is the fractionation constant due to ribulose-1,5-bisphosphate carboxylase-oxygenase (27‰). The constant 0.625 accounts for differences in the diffusion of CO_2 and H_2O .

The BAI was calculated from the measured DBH and annual ring widths. We initially calculated the DBH for each year over the past 30 years by subtracting annual ring widths ($\times 2$) from the DBH at the time of coring (DBH_i). To account for bark thickness we subtracted 1 cm from the measured DBH. The BAI_i was then calculated for each year as follows:

$$\text{BAI}_i = \pi \left(\frac{\text{DBH}_i}{2} \right)^2 - \pi \left(\frac{\text{DBH}_{i-1}}{2} \right)^2$$

Statistical analyses. All data were organized in a PostgreSQL object-relational database and queried for statistical analysis in the R statistical programming language. We used two types of models to test for the effects of spring and autumn timing on resource availability and wood production. The first type of model used all available observations across trees and time. These models tested for the effects of time, spring anomaly and autumn anomaly on BAI, $\delta^{15}\text{N}$ and $\Delta^{13}\text{C}$ from tree rings, and included the main effects of region (GRSM, PRWI, HAFE and CATO) and species (QUAL, QURU and LITU) as blocking factors. Because the different measurements were made at different frequencies, the sample size available for each model varied. For example, $\delta^{15}\text{N}$ was measured every other year but BAI and $\Delta^{13}\text{C}$ were measured every year. Therefore, sample size for comparisons of $\delta^{15}\text{N}$ and BAI (or $\Delta^{13}\text{C}$) was $n = 3,256$, whereas comparisons of BAI and $\Delta^{13}\text{C}$ (no $\delta^{15}\text{N}$) was $n = 6,872$. Observations of spring ($n = 2,143$) and autumn ($n = 2,911$) anomaly were sparse because of low availability of appropriately timed Landsat data. Further, these observations did not always line up with measurements of $\delta^{15}\text{N}$, resulting in $n = 967$ for models comparing spring anomaly with $\delta^{15}\text{N}$ and $n = 1,229$ for models comparing autumn anomaly with $\Delta^{13}\text{C}$.

In our second set of models, we calculated the rate of change (slope) of trends in tree-ring-based measurements over time and compared these rates across sites. These models aid the interpretation of causal relationships between correlated variables identified in the first set of models. Sample sizes for these models equalled the number of sites ($n = 113$). In these models, we also included region and three nominal variables indicating the presence or absence of each of the three tree species at the site, respectively.

To augment exploration of regression statistics in tabular form (Supplementary Tables 1–19), we visualized the relationship between $\delta^{15}\text{N}$ and spring anomaly in scatterplot form (Fig. 3a). To generate Fig. 3a, we first modelled the effects of region and species on $\delta^{15}\text{N}$ (similar to Supplementary Table 4, but lacking spring anomaly). We then modelled the effect of spring anomaly on the model residuals, generating the regression line in Fig. 3a. From the data used to construct this model, we calculated the annual mean spring anomaly and annual mean $\delta^{15}\text{N}$ and present these data in Fig. 3a.

Received 13 April 2016; accepted 8 August 2016;
published 12 September 2016

References

- Schwartz, M. D., Ahas, R. & Aasa, A. Onset of spring starting earlier across the Northern Hemisphere. *Glob. Change Biol.* **12**, 343–351 (2006).
- Jeong, S.-J., Ho, C.-H., Gim, H.-J. & Brown, M. E. Phenology shifts at start vs. end of growing season in temperate vegetation over the Northern Hemisphere for the period 1982–2008. *Glob. Change Biol.* **17**, 2385–2399 (2011).
- Hyvonen, R. *et al.* The likely impact of elevated CO_2 , nitrogen deposition, increased temperature and management on carbon sequestration in temperate and boreal forest ecosystems: a literature review. *New Phytol.* **173**, 463–480 (2007).
- Richardson, A. D. *et al.* Influence of spring and autumn phenological transitions on forest ecosystem productivity. *Phil. Trans. R. Soc. B* **365**, 3227–3246 (2010).
- Keenan, T. F. *et al.* Net carbon uptake has increased through warming-induced changes in temperate forest phenology. *Nat. Clim. Change* **4**, 598–604 (2014).
- Norby, R. J., Warren, J. M., Iversen, C. M., Medlyn, B. E. & McMurtrie, R. E. CO_2 enhancement of forest productivity constrained by limited nitrogen availability. *Proc. Natl Acad. Sci. USA* **107**, 19368–19373 (2010).
- Sigurdsson, B. D., Medhurst, J. L., Wallin, G., Eggertsson, O. & Linder, S. Growth of mature boreal Norway spruce was not affected by elevated CO_2 and/or air temperature unless nutrient availability was improved. *Tree Physiol.* **33**, 1192–1205 (2013).
- Piao, S. L. *et al.* Net carbon dioxide losses of northern ecosystems in response to autumn warming. *Nature* **451**, 49–52 (2008).
- Zaehle, S., Jones, C. D., Houlton, B., Lamarque, J.-F. & Robertson, E. Nitrogen availability reduces CMIP5 projections of twenty-first-century land carbon uptake. *J. Clim.* **28**, 2494–2511 (2015).
- Rustad, L. E. *et al.* A meta-analysis of the response of soil respiration, net nitrogen mineralization, and aboveground plant growth to experimental ecosystem warming. *Oecologia* **126**, 543–562 (2001).
- Campbell, J. L. *et al.* Consequences of climate change for biogeochemical cycling in forests of northeastern North America. *Can. J. Forest Res.* **39**, 264–284 (2009).
- Elmore, A. J., Guinn, S. M., Minsley, B. J. & Richardson, A. D. Landscape controls on the timing of spring, autumn, and growing season length in mid-Atlantic forests. *Glob. Change Biol.* **18**, 656–674 (2012).
- Craine, J. M. *et al.* Global patterns of foliar nitrogen isotopes and their relationships with climate, mycorrhizal fungi, foliar nutrient concentrations, and nitrogen availability. *New Phytol.* **183**, 980–992 (2009).
- McLauchlan, K. K., Craine, J. M., Oswald, W. W., Leavitt, P. R. & Likens, G. E. Changes in nitrogen cycling during the past century in a northern hardwood forest. *Proc. Natl Acad. Sci. USA* **104**, 7466–7470 (2007).
- Bukata, A. R. & Kyser, T. K. Carbon and nitrogen isotope variations in tree-rings as records of perturbations in regional carbon and nitrogen cycles. *Environ. Sci. Technol.* **41**, 1331–1338 (2007).
- Ehleringer, J. R. & Cerling, T. E. Atmospheric CO_2 and the ratio of intercellular to ambient CO_2 concentrations in plants. *Tree Physiol.* **15**, 105–111 (1995).
- Melaas, E. K., Friedl, M. A. & Zhu, Z. Detecting interannual variation in deciduous broadleaf forest phenology using Landsat TM/ETM plus data. *Remote Sens. Environ.* **132**, 176–185 (2013).
- Becklin, K. M., Medeiros, J. S., Sale, K. R. & Ward, J. K. Evolutionary history underlies plant physiological responses to global change since the last glacial maximum. *Ecol. Lett.* **17**, 691–699 (2014).
- Keenan, T. F. *et al.* Increase in forest water-use efficiency as atmospheric carbon dioxide concentrations rise. *Nature* **499**, 324–327 (2013).
- Phipps, R. L. & Whiton, J. C. Decline in long-term growth trends of white oak. *Can. J. Forest Res.* **18**, 24–32 (1988).
- Fenn, M. E. *et al.* Nitrogen excess in North American ecosystems: Predisposing factors, ecosystem responses, and management strategies. *Ecol. Appl.* **8**, 706–733 (1998).
- Frank, D. C. *et al.* Water-use efficiency and transpiration across European forests during the Anthropocene. *Nat. Clim. Change* **5**, 579–583 (2015).

23. Eshleman, K. N., Sabo, R. D. & Kline, K. M. Surface water quality is improving due to declining atmospheric N deposition. *Environ. Sci. Technol.* **47**, 12193–12200 (2013).
24. Steffen, W. *et al.* Planetary boundaries: Guiding human development on a changing planet. *Science* **347** (2015).
25. Duran, J. *et al.* Climate change decreases nitrogen pools and mineralization rates in northern hardwood forests. *Ecosphere* **7**, e01251 (2016).
26. Jonard, M. *et al.* Tree mineral nutrition is deteriorating in Europe. *Glob. Change Biol.* **21**, 418–430 (2015).
27. Aber, J. D. *et al.* Forest processes and global environmental change: predicting the effects of individual and multiple stressors. *Bioscience* **51**, 735–751 (2001).
28. Masek, J. G. *et al.* A Landsat surface reflectance dataset for North America, 1990–2000. *IEEE Geosci. Remote Sens. Lett.* **3**, 68–72 (2006).
29. Elmore, A. J., Mustard, J. F., Manning, S. J. & Lobell, D. B. Quantifying vegetation change in semiarid environments: Precision and accuracy of spectral mixture analysis and the Normalized Difference Vegetation Index. *Remote Sens. Environ.* **73**, 87–102 (2000).
30. McCarroll, D. & Loader, N. J. Stable isotopes in tree rings. *Quat. Sci. Rev.* **23**, 771–801 (2004).

Acknowledgements

Funding provided by the National Aeronautics and Space Administration (no. NNX12AK17G). We thank S.M. Guinn for remote sensing data processing and database development, R. Paulman for dendrochronology and analytical measurements, V. Cunningham and H. Ding for field assistance, D. Taillie for assistance with Fig. 2, and K. McLauchlan for insightful conversation.

Author contributions

A.J.E. and D.M.N. conceived the study, collected the data and oversaw analytical and geospatial measurements. A.J.E., D.M.N. and J.M.C. performed statistical analyses and wrote the manuscript.

Additional information

Supplementary information is [available for this paper](#). Reprints and permissions information is available at www.nature.com/reprints. Correspondence and requests for materials should be addressed to A.J.E.

Competing interests

The authors declare no competing financial interests.